Phytoplankton biomass cycles in the North Atlantic subpolar gyre: A similar mechanism for two different blooms in the Labrador Sea

Léo Lacour[1,2], Hervé Claustre[1,2], Louis Prieur[1,2], and Fabrizio D'Ortenzio[1,2]

[1]Sorbonne Universités, UPMC Université Paris 06, UMR 7093, LOV, Observatoire Océanologique, Villefranche-sur-Mer, France, [2]CNRS, UMR 7093, LOV, Observatoire Océanologique, Villefranche-sur-Mer, France

Abstract An analysis of seasonal variations in climatological surface chlorophyll points to distinct biogeographical zones in the North Atlantic subpolar gyre. In particular, the Labrador Sea appears well delineated into two regions on either side of the 60°N parallel, with very different climatological phytoplankton biomass cycles. Indeed, north of 60°N, an early and short spring bloom occurs in late April, while south of 60°N, the bloom gradually develops 1 month later and significant biomass persists all summer long. Nevertheless, at climatological scale, the first-order mechanism that controls the bloom is identical for both bioregions. The light-mixing regime can explain the bloom onset in both bioregions. In the Labrador Sea, the blooms seem to rely on a mean community compensation irradiance threshold value of 2.5 mol photon $m^{-2} d^{-1}$ over the mixed layer.

1. Introduction

The North Atlantic subpolar gyre experiences large-amplitude phytoplankton biomass cycles with major seasonal blooms [*Longhurst*, 2007]. Future climate change will affect environmental conditions that control bloom dynamics [*Edwards and Richardson*, 2004]. This is one important reason for the recently growing interest toward understanding bloom dynamics and particularly the timing of the bloom that can potentially influence the whole biomass cycle during the remaining productive season [*Henson et al.*, 2006]. The model of *Sverdrup* [1953] describes bloom initiation in spring when the shoaling mixed layer depth (MLD) reaches the so-called critical depth, allowing sufficient light to induce net growth of phytoplankton. This paradigm is consequently still being refined or nuanced [*Lévy*, 2008; *Taylor and Ferrari*, 2011; *Mahadevan et al.*, 2012], confirmed [*Henson et al.*, 2006; *Chiswell*, 2011], and even challenged [*Townsend et al.*, 1992; *Durbin et al.*, 2003; *Behrenfeld*, 2010].

Besides the lack of agreement in the definition of a bloom, part of the ongoing debate might also result from the type of data set used (in situ versus satellite) or from the specific window of observation (local versus regional; annual versus interannual), which might nuance, if not impact, the conclusions. For example, *Henson et al.* [2006] observed clear interannual variability in bloom timing and magnitude in the Irminger Sea, suggesting that several processes probably interact to modulate the bloom. This also pleads for the acquisition of a long time series to extract the "roots" of the observed variability. Similar types of conclusions were reached by *Lavigne et al.* [2013] for a blooming region of the Mediterranean Sea where biophysical mechanisms potentially evident through analysis at the climatological scale were not obvious anymore if the analysis was refocused on specific years. It is more than likely that there is a first-order mechanism driving the bloom in a given region, on which is superimposed the interannual variability of physical forcing modulating the biological response [*Frajka-Williams and Rhines*, 2010]. The corollary is that a robust climatological approach is needed to address the first-order mechanism controlling bloom dynamics in a given region. This is the choice taken in the present analysis which addresses bloom initiation and evolution in the Labrador Sea (LS) as evidenced by climatological time series.

Our specific interest in the LS indeed results from known peculiarities in the bloom phenology (onset, duration, intensity, and decline) in this area. In the northern part (>60°N) of the basin, the bloom starts earlier and is shorter and more intense with respect to the southern part of the basin and more generally to the rest of the North Atlantic subpolar gyre [*Head et al.*, 2000; *Wu et al.*, 2008; *Frajka-Williams and Rhines*, 2010]. This pattern on bloom onset in the LS is paradoxical with observations made by *Siegel et al.* [2002] that show a northward propagation of the spring bloom in the North Atlantic. In the north LS, noticeable
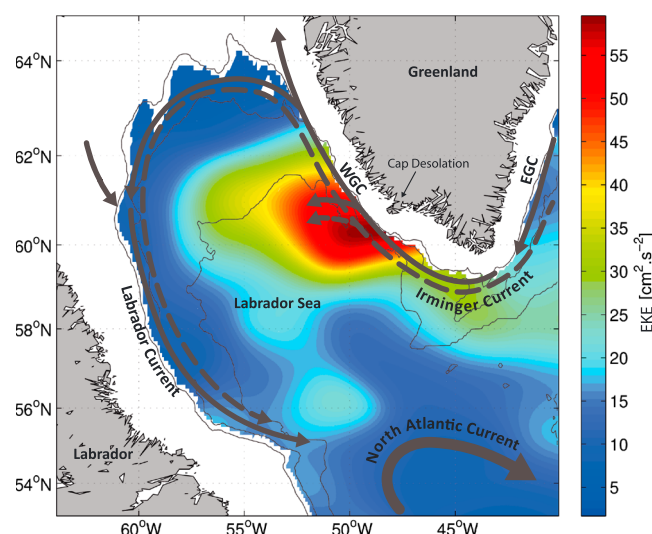
Figure 1. General circulation in the LS superimposed on mean deep eddy kinetic energy (EKE) map (1998–2010) calculated from 1000 m depth Argo float displacement (see Text S1). The dashed arrow corresponds to the Irminger Current extending from 200 to 800 m deep, below the East Greenland Current (EGC), West Greenland Current (WGC), and the Labrador Current that encircles the Labrador Sea. Note the retroflexion of the North Atlantic current south of the basin.

hydrological peculiarities have also been identified. Over the west Greenland shelf, a boundary current, called the West Greenland Current (WGC), carries West Greenland Current Water (WGCW) characterized by cold, fresh water originating from the Arctic at the surface and warm, salty Irminger water of subtropical origin from 300 to 800 m depth. Offshore advection of WGCW occurs off Cap Desolation (~60°N), in a region marked by high eddy kinetic energy (Figure 1). The lateral advection of WGCW, particularly surface fresh water, significantly affects the water column stability in the northern LS [*Hatun et al.*, 2007; *Schmidt and Send*, 2007].

Few studies [*Wu et al.*, 2008; *Frajka-Williams and Rhines*, 2010] have investigated the potential role of haline stratification on phytoplankton phenology. These authors have identified two regions in the LS with a reversed pattern in the bloom onset. *Frajka-Williams and Rhines* [2010] showed that stratification was responsible for the early north LS bloom timing, while light was assumed to control the south LS bloom. *Wu et al.* [2008] also reported an early bloom in the north related to the very shallow mixed layer. Yet they have concluded that light availability plays an important role but is not a determining factor for the early bloom.

Here the paradoxical phenology of the north LS bloom is reinvestigated at climatological scale, with respect to bloom phenology of the subpolar gyre and more particularly of the south LS. First, North Atlantic subpolar gyre regions are identified for their similar bloom phenology (i.e., bioregionalization). Second, this bioregionalization is used to determine, with in situ Argo data, the regional and seasonal variations of water column stability and convolve them with seasonal variations in surface irradiance. This synergetic conjunction of hydrology and surface irradiance, as proposed by the conceptual model of *Sverdrup* [1953], is carried out in order to evaluate the extent to which the bloom phenology in distinct regions is driven by the light-mixing regime.

2. Material and Methods

The bioregionalization of the North Atlantic subpolar gyre (from 40°N to 70°N) was performed according to the method described in *D'Ortenzio and Ribera d'Alcalà* [2009]. The objective of this statistical method is to identify regions with similar patterns in the seasonal cycle of surface chlorophyll a concentration (hereafter called Chl *a*), a proxy of surface phytoplankton biomass. Eight day composite satellite Chl *a* data from the GlobColour project (http://www.globcolour.info) were used to create 8 day climatology (over the 1998–2014 period) for each pixel (spatial resolution of 4 km) of the basin. The GlobColour data set provides a long time series of merged L3 Ocean Colour products from different sensors (Sea-viewing Wide Field-of-view Sensor, Medium-Resolution Imaging Spectrometer, Moderate Resolution Imaging Spectroradiometer Aqua, and Visible Infrared Imaging Radiometer Suite) which ensures data continuity and improves spatial and temporal coverage. A detailed description of the GlobColour product is given in the GlobColour Product User Guide (http://www. globcolour.info/CDR_Docs/GlobCOLOUR_PUG.pdf). To facilitate comparison between pixels, each 8 day value for each pixel was normalized by the maximal and minimal Chl *a* value of each series so that the time series is scaled between 0 and 1. Due to low-incident sun angle in winter, the Chl *a* time series for each pixel lasts only twenty-seven 8 day periods from early March to late September. A cluster K-means analysis [*Hartigan and Wong*, 1979] is then applied, allowing pixels exhibiting similar seasonal cycles of Chl *a* to be assembled.

Each pixel with more than two 8 day periods of missing data is removed from the analysis. The spatial distribution of the different clusters can subsequently be mapped with the associated centroid of each clusters corresponding to the mean seasonal cycle. The number of clusters is set before the analysis and is based on the Calinski and Harabazs index [*Calinski and Harabasz*, 1974; *Milligan and Cooper*, 1985] (see Text S2 and Figure S1 in the supporting information). Here six clusters were used to regionalize the North Atlantic. In the following, the spatial distribution of the cluster is referred to as "bioregion," as proposed by *D'Ortenzio and Ribera d'Alcalà* [2009]. The climatological seasonal phytoplankton biomass cycle associated to each bioregion provides information on timing, duration, and relative intensity of the bloom. The same analysis was also performed on the Labrador Sea alone with only three clusters to better characterize the bioregions in this area (see Figure S2). This region is influenced by the presence of sea ice which could limit the coverage of satellite data during winter period. However, Figure S3 shows that most of the region is free of ice as early as March due, in large part to, the West Greenland Current which carries warm waters of subtropical origin.

In order to analyze more specifically and quantitatively the biomass cycles in the bioregions identified in the LS, new unnormalized 8 day climatological cycles were created by area averaging all Chl *a* data for all pixels of a bioregion (see Figure S2). This pixel selection for area-averaging data within the bioregions is more accurate than a data box selection without any physical or biological meaning.

In this study, the bloom is defined as the rapid accumulation of phytoplankton biomass in the surface layer, seen by satellite. Therefore, the onset is defined here as the maximum accumulation rate *r*, which is expressed as follows:

$$r = \frac{1}{\text{Chl } a} \times \frac{d\text{Chl } a}{dt} \tag{1}$$

Argo data were used to produce monthly climatological time series of area-averaged temperature and salinity within each bioregion of the LS from the surface down to 1000 m depth (see geographic location of Argo data profiles in Figure S4). In the LS, more than 7300 Argo profiles were available for the 1998–2014 period. The accuracy of float data is ±0.002°C in temperature and ±0.005 in salinity. Temperature and salinity profiles were used to estimate the mixed layer depth (MLD) according to the algorithm of *Holte and Talley* [2009] (see supporting information). This algorithm accounts for the vertical density compensation [*De Boyer Montégut et al.*, 2004, Figure 10] that potentially occurs in the LS. A monthly climatological annual cycle of the MLD based on Argo data was estimated for both LS bioregions.

Eight day climatological Photosynthetically Available Radiation (PAR) and PAR diffuse attenuation coefficient (K_{PAR}) were downloaded from the GlobColour website. The PAR was averaged over the mixed layer (PAR_{ML}) to account for the daily amount of photons received by phytoplankton [*Riley*, 1957; *Prieur and Legendre*, 1988; *Morel et al.*, 2010; *Blain et al.*, 2013; *Mignot et al.*, 2014]. This proxy indeed convolves all the processes that control the amount of available light for phytoplankton cells in the water column (i.e., the surface irradiance, the thickness of the layer where phytoplankton is mixed, and the irradiance attenuation within this layer). At short timescale (hours to day), the depth of the turbulent layer which mix phytoplankton cells can be shallower than the mixed layer depth [*Brainerd et al.*, 1995]. Nevertheless, in the climatological context of this analysis, we assumed here that phytoplankton cells are, in average, uniformly distributed throughout the entire mixed layer over the 8 day period. The bloom is supposed to begin when the PAR_{ML} rises above a threshold value called PAR_c. PAR_c, similar to the community compensation irradiance [*Siegel et al.*, 2002], is the mean light energy over the MLD required by photosynthesis to compensate for all loss processes (including mortality and grazing) and to allow for net growth. This approach is based on the concept of *Sverdrup* [1953] but slightly differs from the critical depth hypothesis in the sense that the critical depth Zcr is not used. The underlying concept is that the growth rate is not exponentially decreasing with depth, but rather constant throughout the mixed layer. The PAR below the sea surface [PAR(0−)], was calculated using a reduction of 7.6% of the PAR above the sea surface [PAR(0+)], to take into account the loss by reflection at the air/sea interface [*Morel*, 1991]. The attenuation of PAR with depth was given by the following:

$$\text{PAR}(z) = \text{PAR}(0-) \times \exp(-K_{\text{PAR}} \times z) \tag{2}$$

The mean PAR over the mixed layer was estimated as follows:

$$\text{PAR}_{\text{ML}} = \frac{1}{\text{MLD}} \times \int_0^{\text{MLD}} \text{PAR}(z) \, dz \tag{3}$$

The monthly climatological MLD was linearly interpolated to match 8 day climatological PAR.
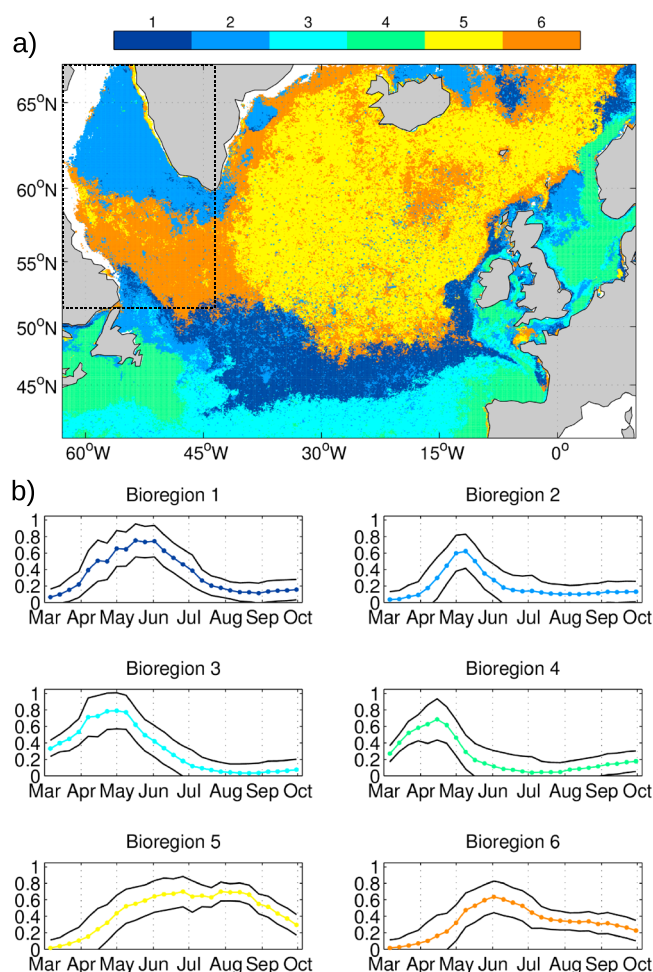
Figure 2. (a) Spatial distribution of the clusters obtained from the K-means analysis and (b) mean normalized Chl *a* annual cycles in each cluster ±1 standard deviation. Each cluster is considered as a bioregion with a spatiotemporal coherence with respect to phytoplankton biomass cycles. The dashed black box delineates the area of interest.
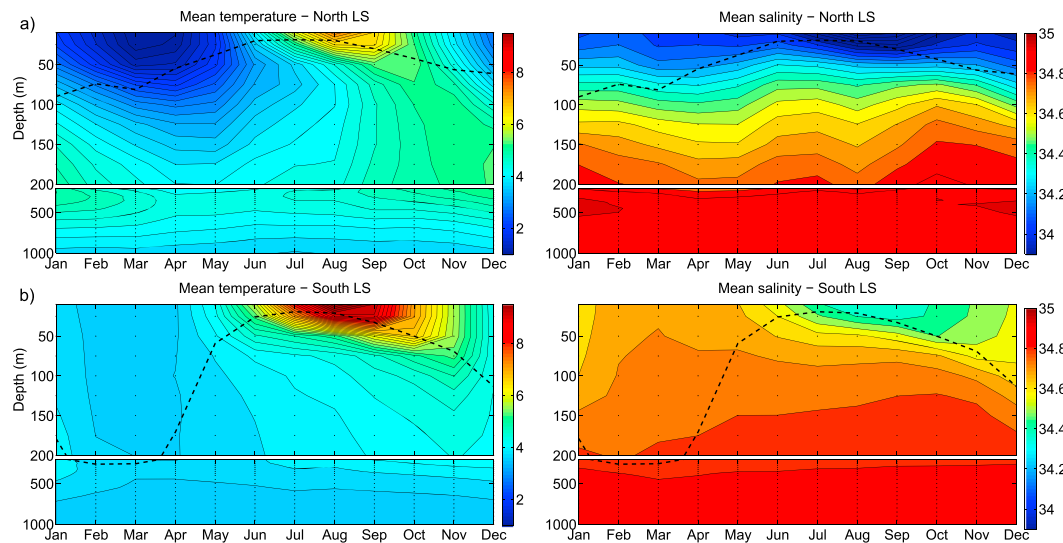
3. Results and Discussion

3.1. Bioregionalization of the North Atlantic With a Focus on the LS

The bioregionalization of the North Atlantic (Figure 2) reveals the high variability of phytoplankton biomass seasonal cycles at a climatological level. Timing, relative intensity, and bloom duration exhibit very significant differences according to bioregions. The cycles associated with bioregions 1 and 3 are typical of temperate regions with the 1 month delay between Chl *a* maxima in both bioregions typically corresponding to the well-known northward propagation of the spring bloom [*Siegel et al.*, 2002]. Bioregion 4, limited to coastal areas, is characterized by an early bloom (maximum biomass in mid-April). Bioregion 5 appears to be well representative of the overall subpolar gyre. It is characterized by a high phytoplankton biomass during 3 months, from June to September. Bioregions 6 and 2 are less spatially coherent than the others, except in the Labrador Sea.

The present bioregionalization of the North Atlantic, only based on satellite Chl *a*, shows similar patterns to the geographical provinces described by *Longhurst et al.* [1995], who also used satellite Chl *a*, as well as *Devred et al.* [2007], who used sea surface temperature and phytoplankton biomass data.

Cluster analysis clearly distinguishes the North Atlantic Drift Province (bioregion 1) in particular the drift retroflection southeast of the LS (Figure 1), the North West Atlantic Shelf Province (bioregion 4), and the Boreal Polar Province (bioregion 2) on the Greenland shelves. However, the pattern is different in the LS with two distinct regions on either side of the 60°N parallel. In particular, the Boreal Polar Province only identified along the Greenland and Labrador shelves by *Longhurst et al.* [1995] and *Devred et al.* [2007] seems to extend into the North Labrador Sea interior as part of the present climatological analysis.

The LS is well separated into two bioregions on either side of the 60°N parallel (Figures 2 and S2). Both bioregions will respectively be referred to as "North LS" (bioregion 2 in Figure S2) and "South LS" (bioregion 3 in Figure S2) In the South LS, the bloom starts in April–May and develops slowly with a relative biomass maximum occurring 2 months later in June. Unexpectedly, in the North LS, a short-duration bloom starts in early April, peaks in May and declines in June (Figure 2b). In the LS, it thus appears that the bloom does not follow an expected latitudinal progression associated with the seasonal increase in surface irradiance [*Siegel et al.*, 2008]. Because of this paradoxical phytoplankton cycle dynamics, the following analysis and discussion will solely focus on the Labrador Sea.

3.2. Climatological Differences in the Hydrological Conditions of the North and South LS

Climatological time series of temperature, salinity, and density, from the surface to 1000 m depth (Figures 3 and S5 for density), clearly evidence different hydrological conditions between both bioregions of the LS

Figure 3. Climatological area-averaged time series of temperature and salinity in the (a) North LS and in the (b) South LS over the 1998–2014 period (see geographic location of the data in Figure S4). Dashed lines denote the climatological MLD. The data (black points) were interpolated using the MATLAB function "contourf." Thin black lines represent contours, with a resolution of 0.2°C for temperature and 0.06 for salinity.

(see bioregions 2 and 3 in Figure S2). The North LS is characterized by cold (~2°C) and fresh (~34.1–34.2) water at the surface from January to June. At intermediate depths (200–800 m), the relatively warm (4–5°C) and salty (~34.9) modified Irminger waters have only been identified in the North LS. These water masses are very similar to the WGCW, especially from December to March. The consequence of the presence of WGCW in the North LS is an increase in the water column stability during winter and early spring [*Head et al.*, 2000]. The MLD in the North LS is indeed at least 100 m shallower than in the South LS over this period.

The fresh and cold upper water layer in the North LS is present during the whole year due to different sources, such as Arctic Ocean water carried by east and west Greenland currents, a high precipitation rate [*DeTracey and Tang*, 1997], or Greenland runoff [*Hanna et al.*, 2008]. All these inputs strongly influence the stability of the water column in the North LS. Climatological buoyancy anomaly has revealed that this region is mostly stratified (MLD < 100 m) due to stabilizing fresh water in spite of destabilizing cold water [*Frajka-Williams and Rhines*, 2010]. In the South LS, the upper water layer is thermally rather than haline stratified from May to November. Before May, solar radiation is too weak to compensate for heat loss, so the MLD is deeper (>400 m).

3.3. Impact of Light and Water Stability on Bloom Onset in the North and South LS

In both bioregions of the LS, very diffe-rent climatological biomass cycles are observed, when addressed quantitatively in terms of Chl *a*. In the North LS, the peak in surface Chl *a* reaches 3.7 mg m^{-3} in late April (Figure 4a), 7 times higher than the value in the South LS at the same period. At the date of the North LS bloom onset (early April; dashed blue line, Figure 4b), the area-averaged surface PAR in the South LS (19 mol photon m^{-2} d^{-1}) is slightly higher than the one in the North LS (16 mol photon m^{-2} d^{-1}; Figure 4c), while the bloom onset in the South LS takes place 1 month later. The thickness of the mixed layer plays a key role on light availability for the development of the bloom in the North LS. Indeed, the mean PAR over the mixed layer (Figure 4d) is twice higher in the North LS than in the South at the same time. In the South LS, the bloom begins 1 month later in early May when PAR$_{ML}$ reaches 2.5 mol photon m^{-2} d^{-1}, the same value that supported the bloom onset in the North LS.

Wu et al. [2008] and *Frajka-Williams and Rhines* [2010] have separately studied the impact of the shoaling of the mixed layer and irradiance (PAR), using the critical depth hypothesis, on the timing of the bloom in the LS. They concluded that the early shoaling was responsible for the early bloom in the North LS, while light controlled the South LS bloom. Both factors are directly linked because the depth of the mixed layer regulates phytoplankton's time exposure to light. The mean PAR over the mixed layer takes the depth of mixing into
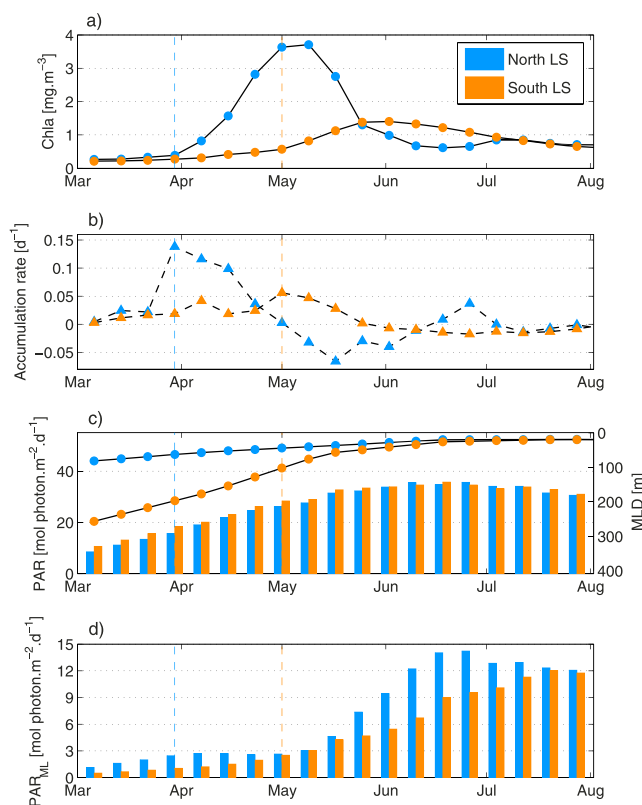
Figure 4. (a) Climatological cycle of area-averaged surface Chl a. Accumulation rate (see equation (1)) of the (b) surface Chl a, (c) surface PAR (bars) and MLD (lines), and (d) mean PAR over the MLD. Vertical dashed lines denote the bloom initiation deduced in Figure 4b. Blue correspond to the North LS and red to the South LS. Note the scale inversion for MLD in Figure 4c. The time axis, from 1 March to 31 July, is centered on the bloom period.

account in the assessment of the light availability (i.e., light-mixing regime). From the present observation, the climatological analysis reveals that the light-mixing regime drives the onset of the bloom in both bioregions of the LS. The mean community compensation irradiance (PAR$_c$) of 2.5 mol photon m^{-2} d^{-1} could be the threshold value that triggers the bloom onset in this region. Interestingly, this value is consistent with the community compensation irradiance of 2.5 mol photon m^{-2} d^{-1} from *Henson et al.* [2006] in the Irminger Sea, 3.5 mol photon m^{-2} d^{-1} from *Riley* [1957] in the Sargasso Sea and of 3 mol photon m^{-2} d^{-1} from *Siegel et al.* [2002] south of 40°N, in stratified environments.

3.4. Bloom Termination and Summer Biomass Evolution

In the North LS, the bloom begins to decline 1 month earlier (early May) and faster than the bloom in the South LS and more generally in the subpolar gyre (early June). It is interesting to analyze the potential causes at the origin of the time shift in bloom decline. Bottom-up (nutrient, light) and top-down (zooplankton, mortality) controls are investigated here.

In most of the North Atlantic, nutrients are replete in early spring to support the bloom onset, thanks to wintertime convection that replenishes upper layers. However, the surface haline barrier in the North LS could limit, at least partially, this wintertime recovery of nutrients. A rapid growth of large phytoplankton cells, such as diatoms, could then lead to a rapid exhaustion of nutrients in the MLD, in particular silicate. This could be amplified by numerous eddies in the North LS which could constitute a net sink of nutrients by vertical advection (for nitrate: 0.01–0.03 mol N m^{-2} yr^{-1} [*McGillicuddy et al.*, 2003]). However, horizontal advection of nutrient-rich Arctic water from the Greenland shelf to the North LS interior seems to compensate for these losses (0.3–1 mol N m^{-2} yr^{-1}). Climatological annual cycles of nitrate and silicate concentrations (World Ocean Atlas 2009), averaged over the MLD in both bioregions of the LS, seem to indicate that nutrient concentrations are weaker in the North LS than in the South LS over a whole year. Nevertheless, these concentrations remain high (Figure S6) especially in the North LS when the bloom starts to collapse. The minimum nutrient concentration indeed occurs in both bioregions in August/September when bloom in the North LS has already collapsed 2 or 3 months before. At climatological scale, nutrients appear to not control the bloom collapse in both bioregions. However, a nitrate profile from a Bio-Argo float in the North LS (data not shown but available at http://www.oao.obs-vlfr.fr/bioargo/PHP/lovbio044b/lovbio044b.html;profile As_120_00) at the end of April 2015 shows a clear nitrate depletion at the surface, associated with very high Chl a (above 10 mg m^{-3}). Thus, on specific years, it appears that nutrient depletion could be at the origin of the North LS bloom collapse.

The possible influence of light limitation on the North LS rapid bloom decline in nutrient-replete conditions has also to be addressed. The high Chl a in a rather thin layer (<50 m) might be at the origin of self-shading and associated inhibition of growth, causing the rapid decline of the bloom [*Marra*, 2004]. PAR$_{ML}$ is a useful

criterion not only to explain bloom initiation but also to evidence a possible light limitation. At climatological scale, PAR_{ML} slightly decreases in the North LS at the time of the maximum Chl a. However, PAR_{ML} never fall below the critical light level (PAR_c) so that light limitation does not appear as first-order explanation of the bloom collapse. Nevertheless, the same analysis performed on specific years shows that PAR_{ML} can fall below the critical light level and leads to the end of the bloom (result not shown). In the South LS, light and nutrients are not a limiting factor but the biomass remains low possibly as a consequence of control by secondary producers.

The top-down control by grazers could indeed influence the phytoplankton biomass cycles in both bioregions of the LS. Nevertheless, the way in which the zooplankton population can regulate the spring bloom still needs to be quantitatively addressed. Observations of annual cycles of zooplankton abundance are rare especially at high latitudes, where in situ data are sparse. According to *Head et al*. [2000], the triggering of reproduction seems to be linked to the start of the spring bloom; however, an early and rapid bloom as in the North LS could lead to a mismatch between primary and secondary producers which, in turn, could explain the high bloom intensity in the North LS compared to the South LS [*Marra and Barber*, 2005; *Ji et al*., 2010]. The establishment of the zooplankton population after the bloom peaks maintains low phytoplankton concentrations in summer despite high light levels.

The mismatch between primary and secondary producers leading to an intense bloom in the North LS could also be at the origin of its abrupt decline. Viral infection is now recognized as a potentially significant cause of phytoplankton mortality [*Lehahn et al*., 2014], resulting in particular in the production of transparent exopolymers. The latter are known to contribute to cell aggregation, enhancing the sinking rate [*Vardi et al*., 2012], and hence the draining of the upper layer from its particulate material.

4. Conclusion

This climatological analysis suggests that the first-order mechanism controlling the initiation of the bloom in both nutrient-replete bioregions of the Labrador Sea is the light-mixing regime, i.e., the concurrent influence of surface light and mixing. The same mechanism can explain two different bloom phenologies. The summer regime still seems to be controlled by grazing or other top-down processes. More generally, this study highlights the importance of in situ measurements to investigate and understand the underlying mechanisms of a complete annual cycle of phytoplankton biomass in remote areas. While satellite remote sensing is essential, it remains nevertheless restricted to the surface layer and thus has to be completed by in situ observations. In particular, it should be noticed that environmental conditions in the North LS are similar to those of the Arctic where a subsurface chlorophyll maximum occurs in summer while it remains unseen by satellites. These data could be nicely complemented by observations of the Bio-Argo type that would resolve interannual variability, as well as reveal the vertical structure of the biological response to physical forcing.

References

Behrenfeld, M. J. (2010), Abandoning Sverdrup's critical depth hypothesis on phytoplankton blooms, *Ecology*, *91*(4), 977–989.

Blain, S., S. Renaut, X. Xing, H. Claustre, and C. Guinet (2013), Instrumented elephant seals reveal the seasonality in chlorophyll and light-mixing regime in the iron-fertilized Southern Ocean, *Geophys. Res. Lett.*, *40*, 6368–6372, doi:10.1002/2013GL058065.

Brainerd, K. E., M. C. Gregg, and F. Sciences (1995), Surface mixed and mixing layer depths, *Deep Sea Res., Part A*, *42*(9), 1521–1543, doi:10.1016/0967-0637(95)00068-H.

Calinski, T., and J. Harabasz (1974), A dendrite method for cluster analysis, *Commun. Stat. Simulat. Comput.*, *3*, 1–27, doi:10.1080/03610917408548446.

Chiswell, S. (2011), Annual cycles and spring blooms in phytoplankton: Don't abandon Sverdrup completely, *Mar. Ecol. Prog. Ser.*, *443*, 39–50, doi:10.3354/meps09453.

D'Ortenzio, F., and M. Ribera d'Alcalà (2009), On the trophic regimes of the Mediterranean Sea: A satellite analysis, *Biogeosciences*, *6*(2), 139–148, doi:10.5194/bg-6-139-2009.

De Boyer Montégut, C., G. Madec, A. S. Fischer, A. Lazar, and D. Iudicone (2004), Mixed layer depth over the global ocean: An examination of profile data and a profile-based climatology, *J. Geophys. Res. Ocean.*, *109*, C12003, doi:10.1029/2004JC002378.

DeTracey, B., and C. L. Tang (1997), Monthly climatological atlas of surface atmospheric conditions of the northwest Atlantic, Can. Data Rep. Hydrogr. Ocean Sci.

Devred, E., S. Sathyendranath, and T. Platt (2007), Delineation of ecological provinces using ocean colour radiometry, *Mar. Ecol. Prog. Ser.*, *346*, 1–13, doi:10.3354/meps07149.

Durbin, E. E. G., R. G. R. Campbell, M. C. M. Casas, M. M. D. Ohman, B. Niehoff, J. Runge, and M. Wagner (2003), Interannual variation in phytoplankton blooms and zooplankton productivity and abundance in the Gulf of Maine during winter, *Mar. Ecol. Prog. Ser.*, *254*(Sverdrup 1953), 81–100, doi:10.3354/meps254081.

Edwards, M., and A. J. Richardson (2004), Impact of climate change on marine pelagic phenology and trophic mismatch, *Nature*, *430*(7002), 881–884, doi:10.1038/nature02808.

Frajka-Williams, E., and P. B. Rhines (2010), Physical controls and interannual variability of the Labrador Sea spring phytoplankton bloom in distinct regions, *Deep Sea Res., Part A*, *57*(4), 541–552, doi:10.1016/j.dsr.2010.01.003.

Hanna, E., P. Huybrechts, K. Steffen, J. Cappelen, R. Huff, C. Shuman, T. Irvine-Fynn, S. Wise, and M. Griffiths (2008), Increased runoff from melt from the Greenland Ice Sheet: A response to global warming, *J. Clim.*, *21*(2), 331–341.

Hartigan, J. A., and M. A. Wong (1979), Algorithm AS 136: A K-means clustering algorithm, *J. R. Stat. Soc. Ser. C Appl. Stat.*, *28*(1), 100–108.

Hatun, C., C. Eriksen, and P. B. Rhines (2007), Buoyant eddies entering the Labrador Sea observed with gliders and altimetry, *J. Phys. Oceanogr.*, *37*(12), 2838–2854.

Head, E. J. H., L. R. Harris, and R. W. Campbell (2000), Investigations on the ecology of *Calanus* spp. in the Labrador Sea: I. Relationship between the phytoplankton bloom and reproduction and development of *Calanus finmarchicus* in spring, *Mar. Ecol. Prog. Ser.*, *193*, 53–73.

Henson, S. A., I. Robinson, J. T. Allen, and J. J. Waniek (2006), Effect of meteorological conditions on interannual variability in timing and magnitude of the spring bloom in the Irminger Basin, North Atlantic, *Deep Sea Res., Part A*, *53*(10), 1601–1615, doi:10.1016/j.dsr.2006.07.009.

Holte, J., and L. Talley (2009), A new algorithm for finding mixed layer depths with applications to Argo data and subantarctic mode water formation, *J. Atmos. Oceanic Technol.*, *26*(9), 1920–1939.

Ji, R., M. Edwards, D. L. Mackas, J. A. Runge, and A. C. Thomas (2010), Marine plankton phenology and life history in a changing climate: Current research and future directions, *J. Plankton Res.*, *32*(10), 1355–1368, doi:10.1093/plankt/fbq062.

Lavigne, H., F. D'Ortenzio, C. Migon, H. Claustre, P. Testor, M. R. d'Alcalà, R. Lavezza, L. Houpert, and L. Prieur (2013), Enhancing the comprehension of mixed layer depth control on the Mediterranean phytoplankton phenology, *J. Geophys. Res. Ocean.*, *118*(7), 3416–3430, doi:10.1002/jgrc.20251.

Lehahn, Y., et al. (2014), Decoupling physical from biological processes to assess the impact of viruses on a mesoscale algal bloom, *Curr. Biol.*, doi:10.1016/j.cub.2014.07.046.

Lévy, M. (2008), The modulation of biological production by oceanic mesoscale turbulence, in *Transport in Geophysical Flow: Ten Years After*, *Lect. Notes Phys.*, edited by J. B. Weiss, and A. Provenzale, pp. 219–261, Springer, Berlin.

Longhurst, A., S. Sathyendranath, T. Platt, and C. Caverhill (1995), An estimate of global primary production in the ocean from satellite radiometer data, *J. Plankton Res.*, *17*, 1245–1271, doi:10.1093/plankt/17.6.1245.

Longhurst, A. R. (2007), Chapter 9—The Atlantic Ocean, in *Ecological Geography of the Sea*, 2nd ed., edited by A. R. Longhurst, pp. 131–273, Academic Press, Burlington.

Mahadevan, A., C. Lee, M. J. Perry, and E. D'Asaro (2012), RESEARCH ARTICLES Eddy-driven stratification initiates North Atlantic spring phytoplankton blooms, *Science*, *337*(6090), 54–58, doi:10.1126/science.1218740.

Marra, J. (2004), The compensation irradiance for phytoplankton in nature, *Geophys. Res. Lett.*, *31*, L06305, doi:10.1029/2003GL018881.

Marra, J., and R. T. Barber (2005), Primary productivity in the Arabian Sea: A synthesis of JGOFS data, *Prog. Oceanogr.*, *65*(2–4), 159–175, doi:10.1016/j.pocean.2005.03.004.

McGillicuddy, D. J., L. A. Anderson, S. C. Doney, and M. E. Maltrud (2003), Eddy-driven sources and sinks of nutrients in the upper ocean: Results from a 0.1° resolution model of the North Atlantic, *Global Biogeochem. Cycles*, *17*(2), 1035, doi:10.1029/2002GB001987.

Mignot, A., H. Claustre, J. Uitz, A. Poteau, F. D'Ortenzio, and X. Xing (2014), Understanding the seasonal dynamics of phytoplankton biomass and the deep chlorophyll maximum in oligotrophic environments: A Bio-Argo float investigation, *Global Biogeochem. Cycles*, *28*, 856–876, doi:10.1002/2013GB004781.

Milligan, G., and M. Cooper (1985), An examination of procedures for determining the number of clusters in a data set, *Psychometrika*, *50*(2), 159–179, doi:10.1007/BF02294245.

Morel, A. (1991), Light and marine photosynthesis: A spectral model with geochemical and climatological implications, *Prog. Oceanogr.*, *26*, 263–306, doi:10.1016/0079-6611(91)90004-6.

Morel, A., H. Claustre, and B. Gentili (2010), The most oligotrophic subtropical zones of the global ocean: Similarities and differences in terms of chlorophyll and yellow substance, *Biogeosciences*.

Prieur, L., and L. Legendre (1988), Oceanographic criteria for new phytoplankton production, *Toward Theory Biol. Phys. Interact. World Ocean*, *239*, 71–112.

Riley, G. A. (1957), Phytoplankton of the North Central Sargasso Sea, *Limnol. Oceanogr.*

Schmidt, S., and U. Send (2007), Origin and composition of seasonal Labrador Sea freshwater, *J. Phys. Oceanogr.*, *37*(6), 1445–1454, doi:10.1175/JPO3065.1.

Siegel, D. A., S. C. Doney, and J. A. Yoder (2002), The North Atlantic spring phytoplankton bloom and Sverdrup's critical depth hypothesis, *Science*, *296*(5568), 730–733, doi:10.1126/science.1069174.

Siegel, D. A., D. B. Court, D. W. Menzies, P. Peterson, S. Maritorena, and N. B. Nelson (2008), Satellite and in situ observations of the bio-optical signatures of two mesoscale eddies in the Sargasso Sea, *Deep Sea Res., Part II*, *55*(10–13), 1218–1230, doi:10.1016/j.dsr2.2008.01.012.

Sverdrup, H. U. (1953), On conditions for the vernal blooming of phytoplankton, *ICES J. Mar. Sci.*, *18*, 287–295.

Taylor, J. R., and R. Ferrari (2011), Shutdown of turbulent convection as a new criterion for the onset of spring phytoplankton blooms, *Limnol. Ocean.*, *56*(6), 2293–2307.

Townsend, D. W., M. D. Keller, M. E. Sieracki, and S. G. Ackleson (1992), Spring phytoplankton blooms in the absence of vertical water column stratification, *Nature*, *360*(6399), 59–62.

Vardi, A., L. Haramaty, B. A. S. Van Mooy, H. F. Fredricks, S. A. Kimmance, A. Larsen, and K. D. Bidle (2012), Host-virus dynamics and subcellular controls of cell fate in a natural coccolithophore population, *Proc. Natl. Acad. Sci. U.S.A.*, *109*(47), 19,327–19,332, doi:10.1073/pnas.1208895109.

Wu, Y., T. Platt, C. C. L. Tang, and S. Sathyendranath (2008), Regional differences in the timing of the spring bloom in the Labrador Sea, *Mar. Ecol. Prog. Ser.*, *355*, 9–20.